Equatorial refuge amidst tropical warming

Kristopher B. Karnauskas* and Anne L. Cohen

Woods Hole Oceanographic Institution

Third revision submitted to *Nature Climate Change* on March 16, 2012

NCLIM–11060505B

*** Corresponding author contact information**

Woods Hole Oceanographic Institution

360 Woods Hole Road, M.S. #23

Woods Hole, MA 02543

(508) 289–3320

kk@whoi.edu

Upwelling across the tropical Pacific Ocean is projected to weaken in accordance with a reduction of the atmospheric overturning circulation[1], enhancing the sea surface temperature (SST) increase relative to other regions in response to greenhouse forcing. In the central Pacific, home to one of the largest Marine Protected Areas (MPAs) and fishery regions in the global tropics, SSTs are projected to increase by 2.8°C by the end of this century[2–4]. Of critical concern is that MPAs may not provide refuge from the anticipated rate of large–scale warming, which could exceed the evolutionary capacity of coral and their symbionts to adapt[5]. Combining high–resolution satellite measurements[6,7], an ensemble of global climate models[4], and an eddy–resolving regional ocean circulation model[8], we show that warming and productivity decline around select Pacific islands will be mitigated by enhanced upwelling associated with a strengthening of the equatorial undercurrent (EUC). Enhanced topographic upwelling will act as a negative feedback, locally mitigating the surface warming. At the Gilbert Islands, the rate of warming will be reduced by 0.7 ± 0.3°C or 25 ± 9% per century, or an overall cooling effect comparable to the local anomaly for a typical El Niño by the end of this century. Since the EUC is dynamically constrained to the equator, only a handful of coral reefs stand to benefit from this equatorial island effect. Nevertheless, those that do face a lower rate of warming, conferring a significant advantage over neighboring reef systems. If realized, these predictions help to identify potential refuges for coral reef communities from anticipated climate changes of the 21st century.

State–of–the–art global climate models predict a weakening of the atmospheric overturning circulation in response to rising levels of atmospheric CO_2[9]. In the tropical Pacific, where the atmosphere and ocean are tightly coupled, a weakening of the trade winds would result in reduced equatorial upwelling and therefore a decline in primary productivity as well as additional warming superimposed on the global mean trend. Both regional changes threaten marine ecosystems. For example, a vast area encompassing one of the world's largest MPAs (the Phoenix Islands Marine Protected Area, PIPA) is projected to warm by up to 2.8°C by the end of this century, a rate of ~0.3°C per decade[2]. This rate of warming cannot be mitigated through local conservation efforts and could be beyond the capacity of most reef–building corals and their algal symbionts to adapt[5]. The west–central Pacific Ocean is also home to the most productive fishery region in the global tropics[10]. Biomass distribution of tuna, which comprise roughly 24% of the total catch in this region[10], are tightly coupled to changes in primary productivity[11,12]. Clearly, these model predictions, if realized, could have dire and irreversible consequences for marine life across the tropical Pacific.

In most cases, however, global climate models do not simulate the interaction of islands and atolls with the mean ocean circulation and therefore do not consider their impact on SST and biomass distribution[13–18]. This effect is documented in Fig. 1, which shows the mean annual surface chlorophyll–*a* concentration (chl hereafter), a proxy for near–surface phytoplankton biomass, for the tropical Pacific as observed by the NASA SeaWiFS satellite[7]. Along the equator, chl gradually increases from ~0.1 mg m^{-3} in the western Pacific to ~0.3 mg m^{-3} in the east, punctuated by the Galápagos Islands, where chl locally exceeds 3 mg m^{-3} (Fig. 1b). The narrow band of high chl along the equator is associated with equatorial upwelling driven by the

easterly trade winds, while the gradual eastward increase in chl mirrors the eastward shoaling of the thermocline and nutricline.

Despite the deeper thermocline and hence lower background chl in the west–central Pacific, a conspicuous enhancement is apparent west of the Gilbert Islands (~174°E), a group of 16 coral atolls forming a line across the equator. Along this transect (3.4°N–2.6°S), eight islands, each exceeding 18 km in length from north to south (twice the resolution of the satellite data) generate an enhancement of chl emanating westward from their shores. By linearly interpolating the chl profile in Fig. 1b between a point immediately east of the Gilberts and the point at which the trade winds reach zero strength (Fig. 1c), it is estimated that the average chl between 2°S–2°N is enhanced by the Gilberts by a maximum of 13% and is detectable up to 1,000 km west of their location.

Although the chl enhancement west of the Gilberts is smaller in magnitude than that of the Galápagos (estimated >200% by the same method, Fig. 1b), the mechanism is similar. The eastward–flowing waters of the EUC, which is dynamically constrained to within ±2° latitude of the equator, are forced to the surface by any island or atoll standing in its path, resulting in a vigorous supply of cold, nutrient–rich water to the euphotic zone. More importantly, it occurs at the western terminus of the equatorial high–productivity band and therefore in a region that would have very low background chl in the absence of the Gilberts. Due to the fortuitous intersection of the Gilberts chain with the equator, productivity is enhanced in the heart of one of the world's most important fisheries.

Nevertheless, global climate models and low–resolution data sets fail to distinguish the Gilberts from the generally warm, oligotrophic western Pacific. Conversely, mean annual SST from high–resolution (4 km) satellite measurements[6] (Fig. 2a) reveal a cross–island SST

difference (δT) owing to a patch of relatively cold water extending ~100 km westward of most of the Gilbert Islands. That the cold patches occur west of the islands and are more pronounced for islands closer to the equator is a clear fingerprint of topographic upwelling of the EUC. At the longitude of the Gilberts (174°E), the eastward velocity of the EUC is maximum on the equator (~57 cm s^{-1}) and tapers to one third of that velocity by 2° poleward[19,20]. The northernmost island (Butaritari, 3.16N°) therefore produces no cold patch, while a smaller island close to the equator (Maiana, 0.94°N) produces a very pronounced one. Since the mean surface current (the South Equatorial Current [SEC]) is westward, the patch of cold, high productivity water is advected westward away from the islands. These interactions, which clearly shape the marine environment surrounding equatorial islands and atolls, are only crudely detectable in a data set with ~28 km resolution[21] (Fig. 2b), and entirely undetectable in a data set with coarser resolution[22] and a global model with grid cells too large to permit islands such as the Gilberts[23] (Fig. 2c–d).

Although global models simulate large–scale changes in SST and ocean currents, they do not presently resolve small topographic features like the Gilbert Islands, and their tropics–wide SST predictions[2–4] may not apply at the local ecosystem level where interactions between islands and ocean circulation are important in shaping the marine environment. Rather, SST projections at the relevant spatial scale require additional information that must be gleaned from high–resolution modeling and satellite observations. To predict the change in SST west of an equatorial island (ΔT_W) where the strength of the EUC influences local SST through topographic upwelling, the mean cross–island SST difference (δT), the sensitivity of δT to the strength of the EUC (m), the predicted change in the strength of the EUC (ΔU), and the predicted change in SST east of the island (ΔT_E) must be known:

$$\Delta T_W = \Delta T_E - m\ \Delta U\ \delta T$$

113 ΔT_E and ΔU are ascertained from 18 global climate models that simulated future
114 emissions scenarios[4]. Under the A2 emissions scenario, ΔT_E is projected to rise steadily, reaching
115 ~2.8°C by the 2090s (Fig. 3a). In the same simulations, the surface current (*i.e.,* the SEC)
116 weakens and the EUC strengthens (Fig. 3b–c). Comparing the last decade of the 21st century in
117 the A2 simulation with the 1990s decade of the 20th century simulation, and considering those
118 nine models whose EUC best replicates observations[24], the median projection for the SEC (EUC)
119 is a 15.2% weakening (14.4% strengthening). The weakening of the SEC is consistent with the
120 weakening of the Walker circulation and easterly trade winds[1,9], and hence projections of
121 enhanced warming in the central tropical Pacific relative to other regions[2,3]. The dynamics
122 driving a stronger EUC despite weaker trade winds and SEC is the same as those governing the
123 regular annual cycle in the tropical Pacific, which is well documented[25].
124 Given the lack of sufficient spatial resolution in global models to resolve small islands
125 and the present inadequacy of satellite or *in situ* time series to assess δT and ΔU covariability,
126 estimating the slope parameter m requires a separate numerical simulation of the tropical Pacific
127 Ocean with high–enough resolution to adequately represent the Gilbert Islands and their
128 interaction with equatorial circulation (see Methods). The mean and annual cycle of the EUC is
129 well represented in this eddy–resolving simulation, which leads a statistically robust annual cycle
130 in the simulated δT (Fig. 4). Based on this simulation, we estimate the slope parameter m to be
131 6.0. δT is estimated from high–resolution satellite observations[6] (here we use 0.8°C).
132 In our high–resolution simulation, topographic upwelling velocity is an exponential
133 function of the EUC (r^2=0.84); this model predicts a 50.1% increase in topographic upwelling
134 velocity given a 14.4% increase in EUC strength. The implication for islands like the Gilberts is
135 that a negative feedback driven by the increased topographic upwelling of EUC water will

136 become stronger and at least partially offset the tendency for rising SSTs caused by the enhanced
137 atmospheric greenhouse effect and reduced equatorial upwelling (Fig. 5). For the projected
138 changes in SST and the EUC under the A2 emissions scenario, the warming west of the Gilberts
139 will be indistinguishable from the regional warming or warming east of the islands due to the
140 lack of change in the EUC until ~2030. After 2030, the warming west of the Gilberts will be
141 reduced by a steadily widening margin that exceeds 0.5°C by late 21st century. Given the
142 significant influence of natural climate variability in the central equatorial Pacific Ocean on
143 subseasonal, interannual (*i.e.*, ENSO), and decadal time scales, we compare the projected cooling
144 effect with the range of natural SST variability at those frequencies (Fig. 5, green/yellow error
145 bars). Indeed, the mitigating influence of enhanced upwelling will surpass natural variability due
146 to ENSO as a first order influence by the end of this century. More than 20% of the warming
147 projected for this location in the absence of the island–EUC interaction (or the warming east of
148 the island) will be mitigated by this effect, remaining steady after mid–century even as regional
149 SSTs continue to rise. In addition, the cross–island SST difference (δT) will increase at a rate of
150 0.7 ± 0.3°C per century (uncertainty bounds correspond to ± 2 standard errors of the multi–
151 model mean projected change in EUC strength), a trend that is within error of the observed trend
152 in δT between 1982–2010[21], which we estimate to be 0.43°C per century by differencing trends
153 in the two boxes shown in Fig. 2b.

154 One obvious benefit for the coral reefs of the equatorial Gilbert Islands will be a reduced
155 rate of warming relative to that expected from coarse resolution model projections. This effect
156 should be strongest on the western sides of the Gilberts where the topographic upwelling occurs.
157 Moreover, we can expect the climate–model projected changes in vertical stratification[26] to
158 increase the efficiency of this upwelling to cool the mixed layer. Relatively short–term extreme

warming events (El Niño), during which widespread coral bleaching has been observed[27], will still occur but superimposed on a cooler mean state than that which would exist without this equatorial island effect. In terms of the regional–scale distribution of phytoplankton biomass, the strengthening EUC combined with the weakening SEC should result in increased chl locally, even if weaker background upwelling associated with the trade winds dominates the response of the basin–wide tongue of high productivity.

A few other tropical islands and coral atolls stand to benefit from this equatorial island effect. By virtue of being directly on the path of the EUC, the Galápagos Archipelago may too be spared some of the ecological effects of reduced upwelling projected for the tropical Pacific. Other coral reef systems within the cool stream of the EUC include Jarvis Island (U.S., Central Line Islands), Howland and Baker Islands (U.S.), Banaba Island (Republic of Kiribati), and Nauru Island. Although smaller than the Gilberts, many of these islands are situated further to the east where the thermocline is shallower, the EUC stronger, and therefore the mean cross–island SST contrast and potential natural mitigation greater. If the climate model projection of a weaker Walker circulation and associated wind–driven equatorial upwelling is realized, these equatorial islands could become refuges for marine productivity and coral reefs in an otherwise desolate tropical seascape.

177 **Methods**

178 To estimate the slope parameter *m*, we ran a high–resolution numerical ocean model
179 simulation based on the widely–used Regional Ocean Modeling System (ROMS)[8], distributed
180 along with the pre/post–processing MATLAB toolbox[28] by the French group L'Institut de
181 recherche pour le développement (IRD). Designed specifically for high–resolution simulations of
182 regional domains, ROMS is a free–surface, terrain–following coordinate ocean model that solves
183 the primitive equations in an Earth–centered, rotating frame of reference. The domain of our
184 simulation included the full width of the tropical Pacific Ocean from 130°E–70°W, from 20°S–
185 20°N, with 32 vertical levels. For simplicity, open boundaries were used along the western,
186 southern, and northern boundaries of the domain, and a realistic representation of the American
187 continental coastline closed off the eastern boundary. The horizontal resolution in our simulation
188 was a uniform 1/14° latitude by longitude, or 7.8 km^2. The total size of our domain was thus
189 2,239 x 571 x 32, or ~41 million grid points. Parallel processing was implemented through the
190 MPI protocol on a distributed–memory linux cluster. Our domain was partitioned into 28 x 9
191 tiles, which were integrated simultaneously on 21 nodes (252 cores). A total span of 15 years (5
192 years spin–up, 10 years for analysis) was simulated with a 20–minute model time step, saving
193 monthly average output fields. The 15–year simulation took roughly 3.3 days to complete.

194 To represent a typical Gilbert island, a 5 x 5 (39 km^2) island was placed on the equator
195 centered on 174°E. Our simulation did not use heat flux correction, which is a scheme that
196 adjusts heat fluxes so as to relax the model SST field toward observed values. The ocean model
197 simulates a mean annual cross–island SST difference δT of about 0.14°C and a seasonal
198 maximum δT of 0.49°C. This simulated δT is of the same order of magnitude as that estimated
199 from high–resolution satellite observations but with a low bias. Estimation of the parameter *m*

200 was achieved by isolating the annual signal of the simulated EUC just west of the island and that
201 of the simulated δT and computing the ratio of their amplitudes.
202

203 **References and Footnotes**

204 1. Vecchi, G.A. and B.J. Soden, 2007: Global warming and the weakening of the tropical
205 circulation. *J. Climate*, **20**(17), 4316–4340.

206 2. Clement, A.C., A.C. Baker, and J. Leloup, 2010: Patterns of tropical warming. *Nature*
207 *Geoscience*, **3**, 8–9, doi:10.1038/ngeo728

208 3. Xie, S.–P., C. Deser, G.A. Vecchi, J. Ma, H. Teng, and A.T. Wittenberg, 2010: Global
209 warming pattern formation: Sea surface temperature and rainfall. J. Climate, 23, 966–
210 986.

211 4. Solomon, S., D. Qin, M. Manning, M. Marquis, K. Averyt, M. M. B. Tignor, H. L. Miller, and
212 C. Zhenlin, Eds., 2007: Climate Change 2007: The Physical Science Basis. Cambridge
213 University Press, 996 pp.

214 5. Hughes, T., A. Baird, D. Bellwood, M. Card, S. Connolly, C. Folke, R. Grosberg, O. Hoegh–
215 Guldberg, J. Jackson, J. Kleypas, J. Lough, P. Marshall, M. Nyström, S. Palumbi, J.
216 Pandolfi, B. Rosen and J. Roughgarden, 2003: Climate change, human impacts, and the
217 resilience of coral reefs. *Science*, **301**, 929–933.

218 6. Esaias, W. E., Abbott, M. R., Barton, I., Brown, O. B., Campbell, J. W., Carder, K. L., Clark,
219 D. K., Evans, R. H., Hoge, F. E., Gordon, H. R., Balch, W. M., Letelier, R., and P. J.
220 Minnett, 1998: An overview of MODIS capabilities for ocean science observations. *IEEE*
221 *Transactions on Geoscience and Remote Sensing*, **36**(4), 1250–1265.

222 7. McClain, C. R., G. C. Feldman, and S. B. Hooker, 2004: An overview of the SeaWiFS project
223 and strategies for producing a climate research quality global ocean bio–optical time
224 series. *Deep–Sea Res. II*, **51**, 5–42. Data from the full SeaWiFS mission are used
225 (9/1997–8/2010). Downloaded from NASA Giovanni server.

8. Shchepetkin, A. F., and J. C. McWilliams (2005), The Regional Ocean Modeling System: A split–explicit, free–surface, topography–following coordinates ocean model, *Ocean Modell.*, **9**, 347–404, doi:10.1016/j.ocemod.2004.08.002.

9. Vecchi, G.A., B.J. Soden, A.T. Wittenberg, I.M. Held, A. Leetmaa, and M.J. Harrison, 2006: Weakening of tropical Pacific atmospheric circulation due to anthropogenic forcing, *Nature*, **441**(7089), 73–76.

10. The State of World Fisheries and Aquaculture 2008. Fisheries and Aquaculture Department, Food and Agriculture Organization of the United Nations. Copyright FAO, Rome, 2009. 176 p.

11. Laurs, R.M., P.C. Fiedler, and D.R. Montgomery, 1984: Albacore tuna catch distributions relative to environmental features observed from satellites. *Deep–Sea Res.*, **31**(9), 1085–1099.

12. Pauly, D., and V. Christensen, 1995: Primary production required to sustain global fisheries. *Nature*, **374**, 255–257.

13. Xie, S.–P., W.T. Liu, Q. Liu and M. Nonaka, 2001: Far–reaching effects of the Hawaiian Islands on the Pacific Ocean–atmosphere system. *Science*, **292**, 2057–2060.

14. Feldman, G.C., D. Clark, and D. Halpern, 1984: Satellite color observations of the phytoplankton distribution in the eastern Equatorial Pacific during the 1982–83 El Niño. *Science*, **226**, 1069–1071.

15. Eden, C. and A. Timmermann, 2004: The influence of the Galápagos Islands on tropical temperatures, currents and the generation of tropical instability waves. *Geophys. Res. Lett.*, **31** (L15308) doi:10.1029/2004GL020060

16. Karnauskas, K.B., R. Murtugudde, and A.J. Busalacchi, 2007: The effect of the Galápagos Islands on the equatorial Pacific cold tongue. *J. Phys. Oceanogr.*, **37**(5), 1266–1281.

17. Gove, J. M., M. A. Merrifield, and R. E. Brainard, 2006: Temporal variability of current–driven upwelling at Jarvis Island, *J. Geophys. Res.*, **111**, C12011, doi:10.1029/2005JC003161.

18. Messié, M., M.–H. Radenac, J. Lefèvre, and P. Marchesiello, 2006: Chlorophyll bloom in the western Pacific at the end of the 1997–1998 El Niño: The role of the Kiribati Islands, *Geophys. Res. Lett.*, **33**, L14601, doi:10.1029/2006GL026033.

19. Carton, J.A., and B.S. Giese, 2008: A Reanalysis of Ocean Climate Using Simple Ocean Data Assimilation (SODA). *Mon. Wea. Rev.*, **136**, 2999–3017.

20. Johnson, G.C., B.M. Sloyan, W.S. Kessler, and K.E. McTaggart, 2002: Direct measurements of upper ocean currents and water properties across the tropical Pacific Ocean during the 1990's. *Progr. Oceanogr.*, **52**(1), 31–61.

21. Reynolds, R. W., T. M. Smith, C. Liu, D. B. Chelton, K. S. Casey and M. G. Schlax, 2007: Daily High–resolution Blended Analyses for sea surface temperature. *J. Climate*, **20**, 5473–5496.

22. Reynolds, R.W., N.A. Rayner, T.M. Smith, D.C. Stokes, and W. Wang, 2002: An improved in situ and satellite SST analysis for climate. *J. Climate*, **15**, 1609–1625.

23. Wittenberg, A.; Rosati, Anthony; Lau, Ngar–Cheung; Ploshay, and J. Jeffrey, 2006: GFDL's CM2 global coupled climate models—Part 3: Tropical Pacific Climate and ENSO. *J. Climate*, **19**(5): 698–722. doi:10.1175/JCLI3631.1.

24. Karnauskas, K.B., G.C. Johnson, and R. Murtugudde, 2012: An equatorial ocean bottleneck in global climate models. *J. Climate*, **25**, 343–349.

271 25. Philander, S. G. H., W. J. Hurlin, and A. D. Seigel, 1987: Simulation of the seasonal cycle of
272 tropical Pacific Ocean. *J. Phys. Oceanogr.*, **17**, 1986–2002.
273 26. DiNezio, Pedro N., Amy C. Clement, Gabriel A. Vecchi, Brian J. Soden, Benjamin P.
274 Kirtman, Sang–Ki Lee, 2009: Climate Response of the Equatorial Pacific to Global
275 Warming. *J. Climate*, **22**, 4873–4892.
276 27. Donner, S.D., T. Kirata, and C. Vieux (in press) Recovery for 2004–2005 mass coral
277 bleaching in the Gilbert Islands, Kiribati. Atoll Research Bulletin.
278 28. Penven, P., P. Marchesiello, L. Debreu, and J. Lefevre, 2008: Software tools for pre– and
279 post–processing of oceanic regional simulations. *Environ. Modell. Software*, **23**, 660–
280 662.
281 29. SeaWinds sensor on NASA QuikSCAT satellite, 2000–2008, 1/4° spatial resolution, acquired
282 from IFREMER/CERSAT.
283 30. Smith, T.M., R.W. Reynolds, T.C. Peterson, and J. Lawrimore, 2008: Improvements to
284 NOAA's Historical Merged Land–Ocean Surface Temperature Analysis (1880–2006).
285 *Journal of Climate*, **21**, 2283–2296.
286

Corresponding Author Kristopher B. Karnauskas, Department of Geology & Geophysics, Woods Hole Oceanographic Institution, 360 Woods Hole Road, M.S., #23. Woods Hole, MA, 02536, USA, 508–289–3320, kk@whoi.edu.

Acknowledgements We thank the U.S. National Science Foundation for support, and Delia Oppo and Raghu Murtugudde for reading and providing comments on a draft of the manuscript. Ocean color data were acquired through the National Aeronautics and Space Administration (NASA) Ocean Color Giovanni web site. IPCC climate model outputs were acquired from the World Climate Research Program (WCRP) Coupled Model Intercomparison Project 3 (CMIP3) archive, hosted by the Lawrence Livermore National Laboratory (LLNL). Optimal Interpolation sea surface temperature data sets were acquired from the National Oceanic and Atmospheric Administration (NOAA) National Climate Data Center (NCDC) FTP portal. The Regional Ocean Modeling System (ROMS) code, including the ROMSTOOLS MATLAB toolbox, was generously provided by L'Institut de recherche pour le développement (IRD) on their web site (http://roms.mpl.ird.fr).

Author Contributions K.B.K. acquired and analyzed the global observational data sets and IPCC climate model outputs, and conducted the high–resolution regional ocean model simulation. K.B.K. and A.L.C. discussed the results and biological implications and wrote the paper together.

Author Information All data sets were downloaded freely from the data bases mentioned in the Acknowledgements statement. Subsetted data and/or MATLAB codes are available upon request

310 to the authors. Reprints and permissions information are available at www.nature.com/reprints.
311 The authors declare no competing financial interests. Correspondence and requests for materials
312 should be addressed to K.B.K. (kk@whoi.edu).
313

Figure Legends

Figure 1: Chlorophyll across the equatorial Pacific. (A) Mean annual surface chl–*a* concentration (mg m^{-3}) in the equatorial Pacific Ocean[7] (note that the latitude dimension is stretched relative to longitude). (B) Profile of (A) averaged between 2°S–2°N. (C) Profile of mean annual easterly wind stress (10^{-2} Pa) along the equator[29]. Chl–a data in (B) within the longitudinal range of the Gilbert Islands are omitted. The thin black line near the Gilberts linearly interpolates between the first data point east of the Gilbert Islands and the data point at the longitude where zonal wind stress equals zero (155°E). A similar method is applied to the Galápagos Islands. It is assumed that the islands are responsible for the integral differences between the linear interpolations and the measurements, indicated by the light green shaded regions. The Chl anomaly due to the Gilberts is distinguishable 5–10° longitude or 500–1,110 km westward).

Figure 2: Sea surface temperature near the Gilbert Islands. Mean annual SST centered on the Gilbert Islands (4°S–4°N x 166°E–180°W) from three observational data sets[6,21,22] and one representative CMIP3/IPCC AR4–class global climate model[23]. Spatial resolution (longitude × latitude) is indicated in the upper–right corner of each panel. Each panel includes a dashed line connecting the 9 major Gilbert Islands ($\Delta y > 18$ km) and a solid horizontal line marking the equator. The two boxes shown in (B) indicate locations used in the calculation of observed trends between 1982–2010. In (A)–(C), mean annual SST was computed over the period 2000–2007 for consistency with the Terra MODIS mission (A). In (D), mean annual SST was computed from the first 8 years of the SRES–A1B/run1 output of the GFDL CM2.1 model. Color scales vary between panels due to biases; SST values in (A) span ~28.6°C–29.7°C.

Figure 3: Global climate model projections. Changes at 174°E, 0°N in SST (A), the westward surface current (B), and the eastward undercurrent (C) throughout the A2 simulations by 18 CMIP3/IPCC AR4–class global climate models[4]. In (A), ΔSST is expressed as the absolute departure from the 2000s decade mean, while in (B) and (C), changes in ocean currents are expressed as the percent change relative to each model's own 2000s decade mean. In each panel, the heavy black line (error bars) represents the multi–model mean (interquartile range).

Figure 4: An eddy–resolving regional model simulation. Power spectra (top row) and annual cycle fit to the raw time series (middle row) of the strength of the equatorial undercurrent at 174°E, 0°N (EUC; left column) and the cross–island SST difference (δSST; right column) simulated by a regional ocean model with 8–km resolution[8]. 99% confidence limits, shown as dashed lines in the top row, are based on 10^6 randomly generated time series, each having the same lag–1 autocorrelation as the original time series. The mean is removed from each time series in the middle row. The bottom panel directly compares the annual cycles from the middle row after scaling by the standard deviation; δSST lags the EUC by 1–2 months.

Figure 5: Projected changes in local SST at the Gilbert Islands. Projected changes in (A) SST west relative to east of the Gilbert Islands (or, equivalently, the projection of the cross–island δSST) and (B) percent mitigation of SST change west relative to east of the Gilbert Islands based on the linear inverse model described in the text. Gray error bars in (A) indicate the interquartile range of 18 models. Blue (red) lines indicate the sensitivity of the predictions to increasing (decreasing) one (solid) or both (dashed) of the model parameters m and δT by 25%. The dark

green, light green, and yellow error bars on the left side of (A) indicate the magnitude of SST variations at 174°W, 0°N associated with ENSO, decadal variability, and subseasonal ocean noise, respectively. The green error bars extend ±1 standard deviation of detrended 7–year high–pass filtered SST anomalies for ENSO and 10–year low–pass filtered SST anomalies for decadal variability from observations spanning 1900–2011[30], and the yellow error bar extends ±1 standard deviation of simulated SST anomalies from the high–resolution ocean model simulation forced with climatological boundary conditions.

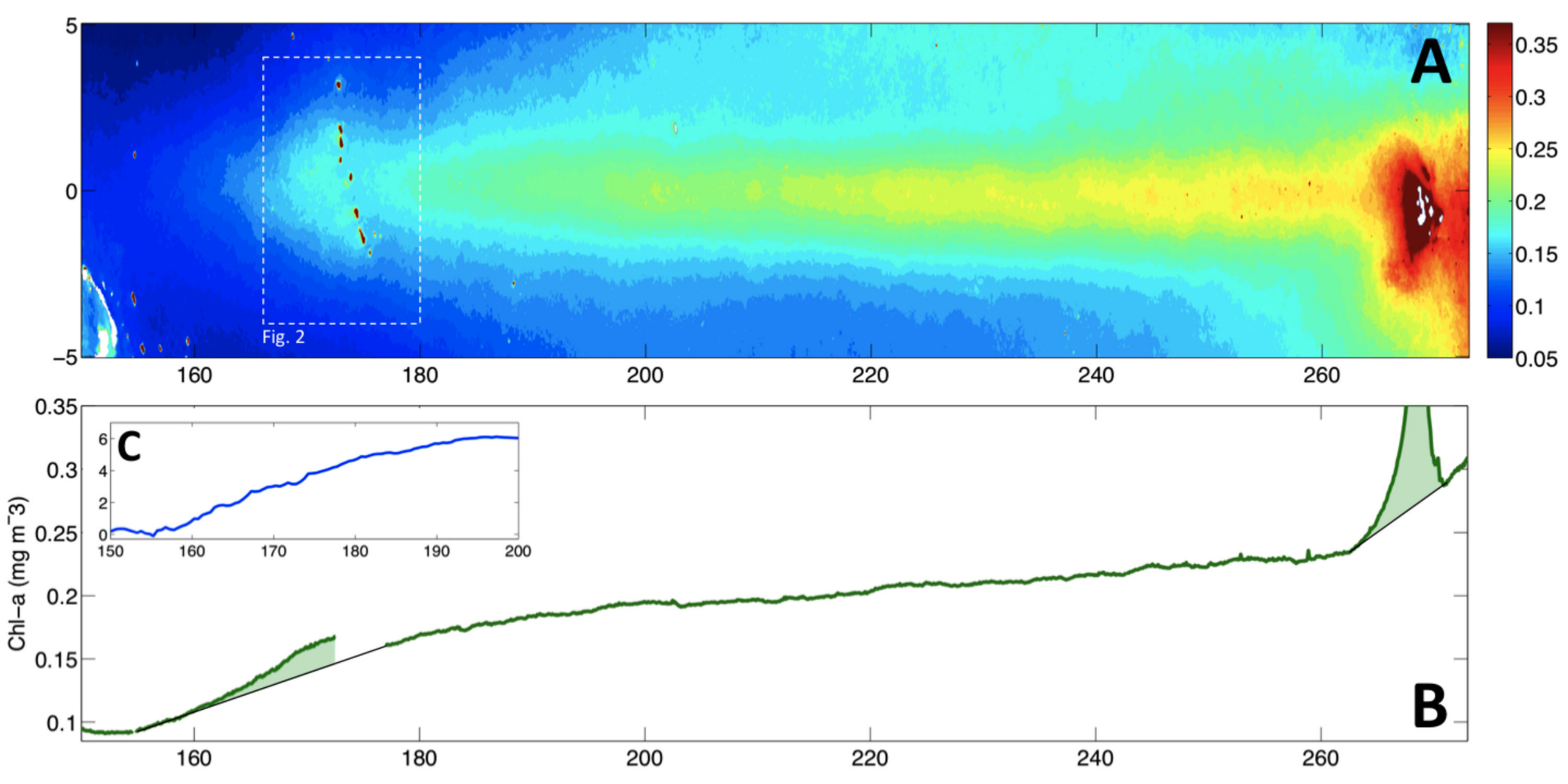
A
Fig. 2
5
0
−5
160
180
200
220
240
260
0.35
0.3
0.25
0.2
0.15
0.1
0.05
B
C
Chl–a (mg m^-3)
0.35
0.3
0.25
0.2
0.15
0.1
6
4
2
0
150
160
170
180
190
200

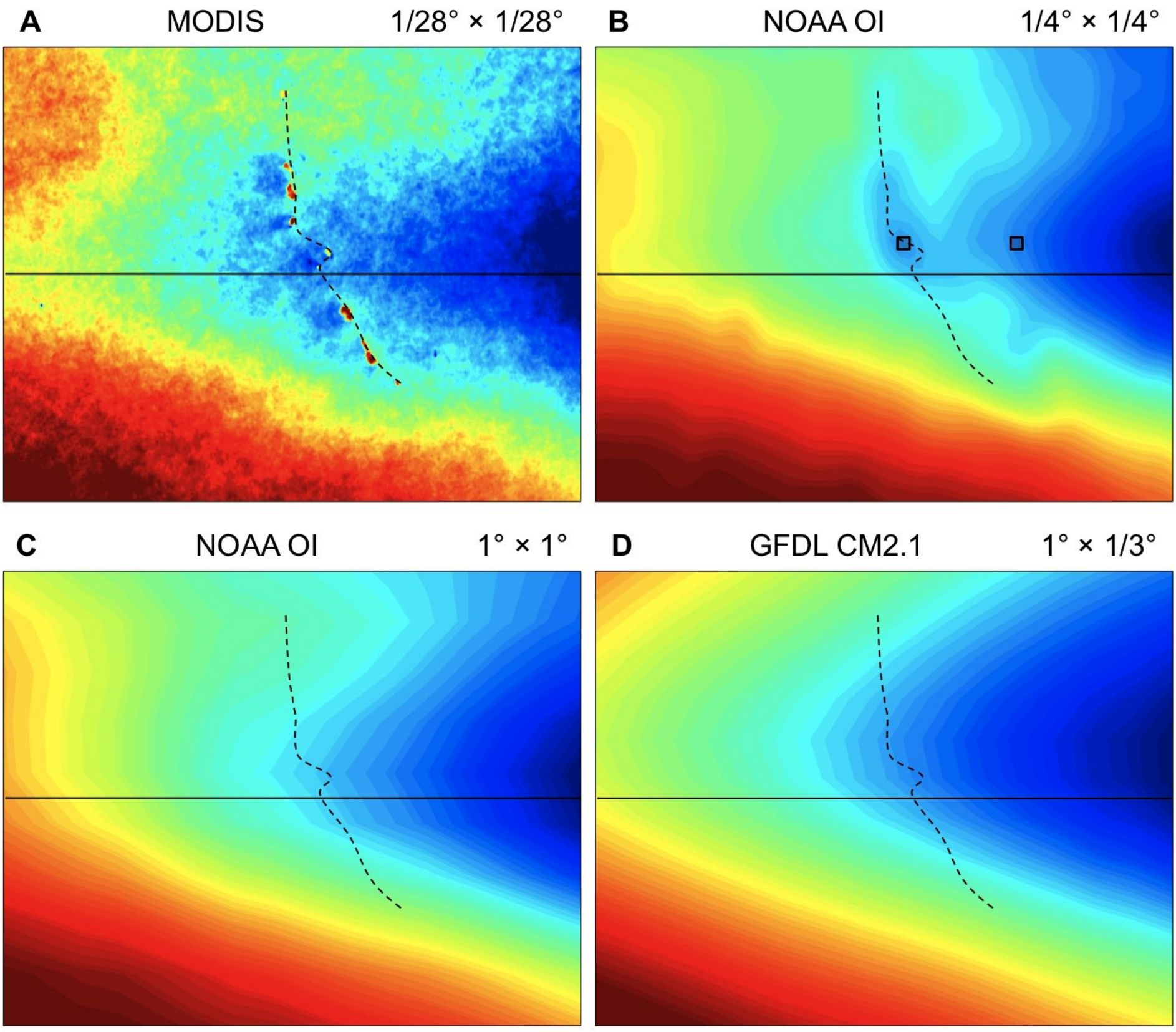
A
MODIS
1/28° × 1/28°
B
NOAA OI
1/4° × 1/4°
C
NOAA OI
1° × 1°
D
GFDL CM2.1
1° × 1/3°

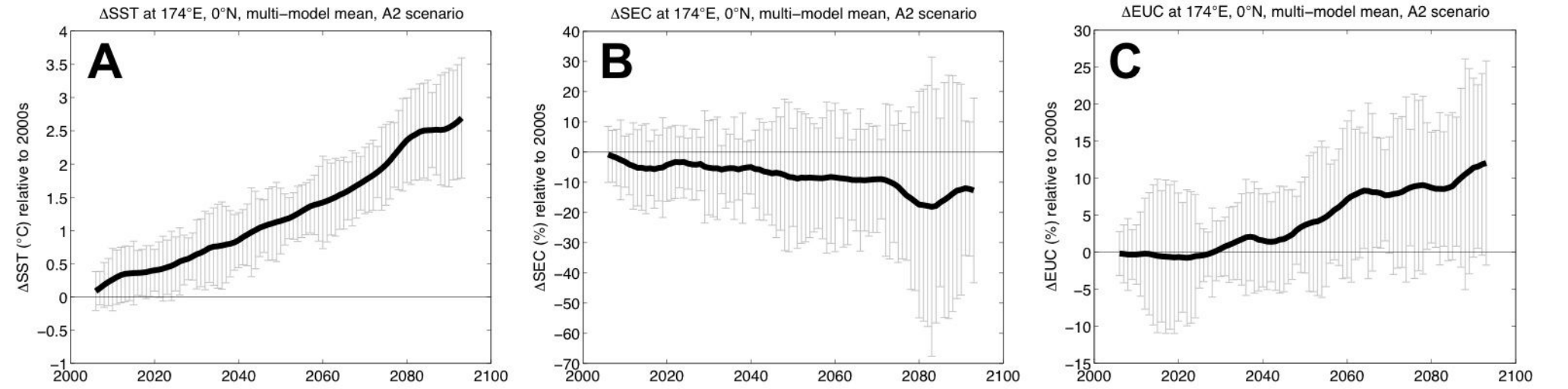
ΔSST at 174°E, 0°N, multi−model mean, A2 scenario
A
ΔSST (°C) relative to 2000s
ΔSEC at 174°E, 0°N, multi−model mean, A2 scenario
B
ΔSEC (%) relative to 2000s
ΔEUC at 174°E, 0°N, multi−model mean, A2 scenario
C
ΔEUC (%) relative to 2000s
2000
2020
2040
2060
2080
2100

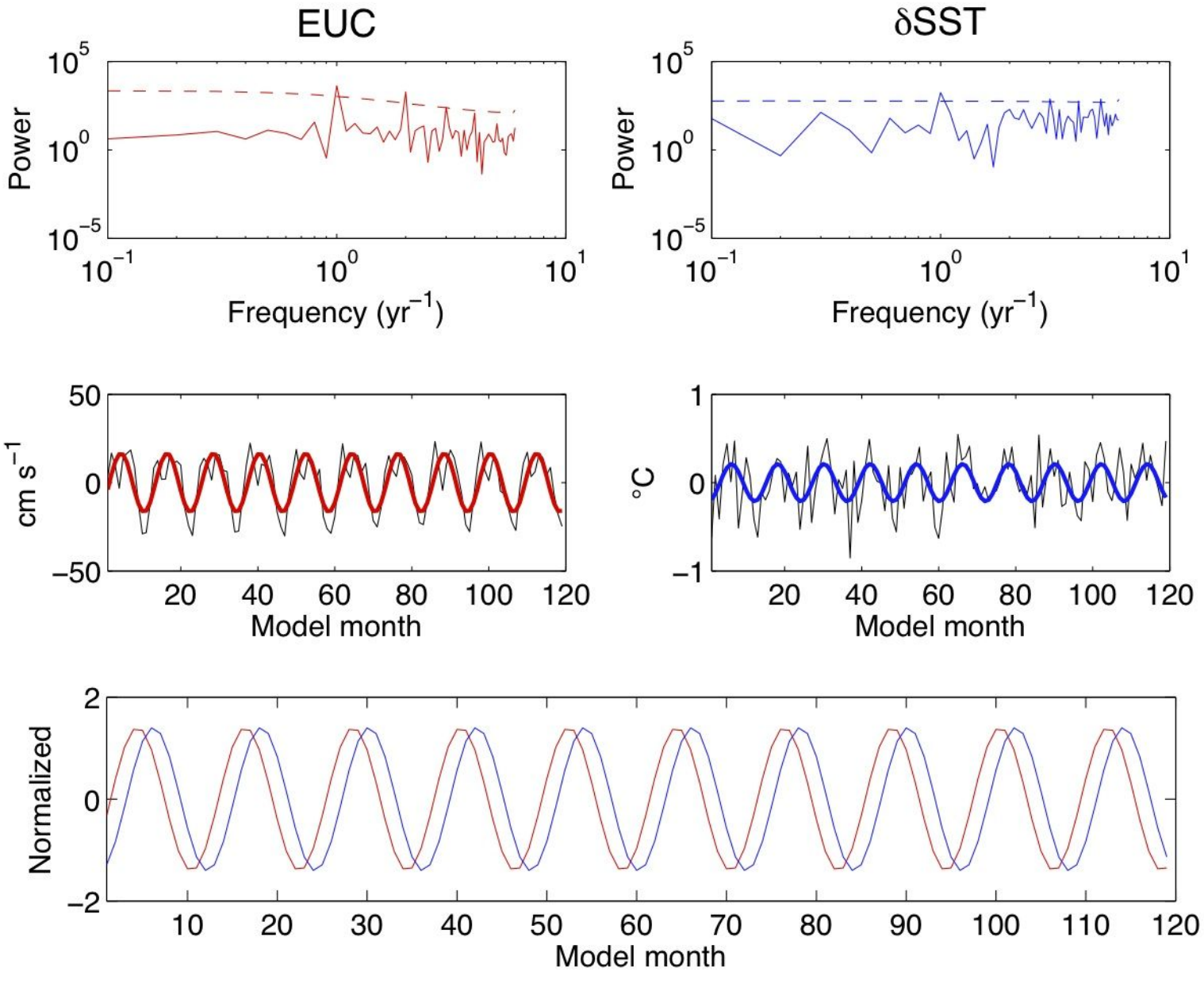
EUC
δSST
Power
Frequency (yr^{-1})
cm s^{-1}
°C
Model month
Normalized

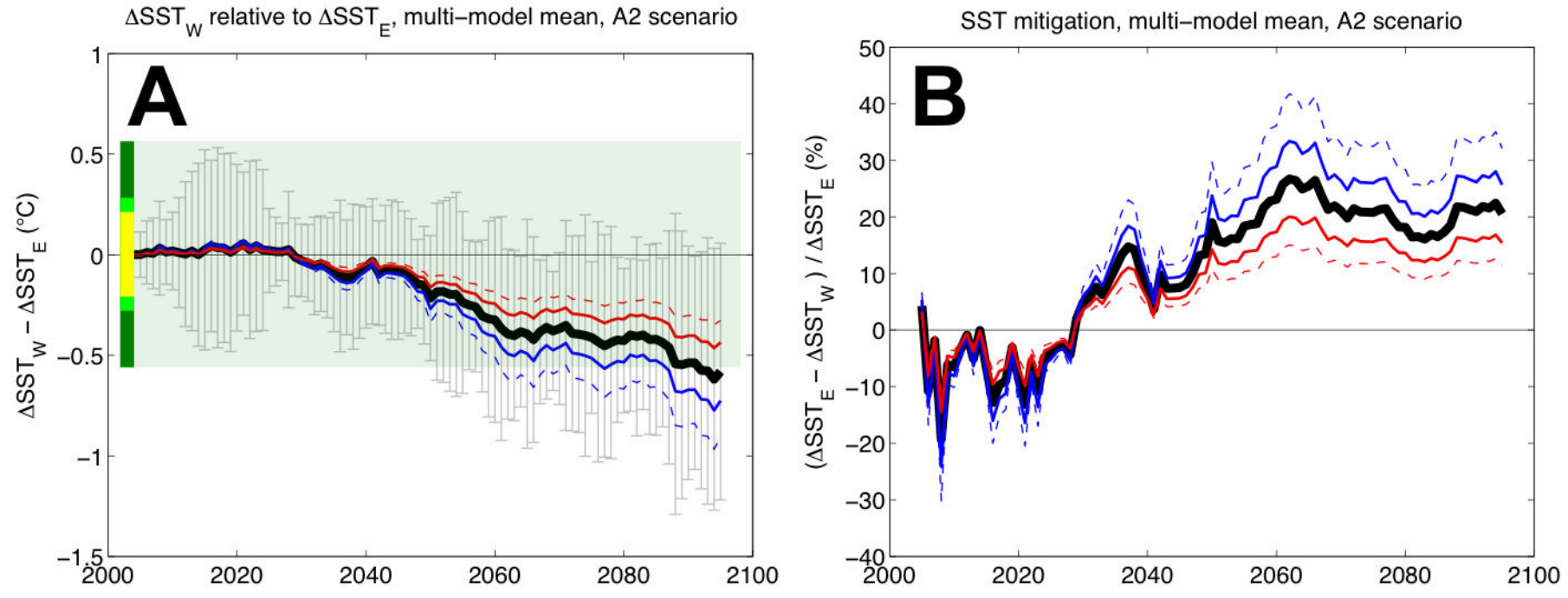
ΔSST_W relative to ΔSST_E, multi−model mean, A2 scenario
A
ΔSST_W − ΔSST_E (°C)
1
0.5
0
−0.5
−1
−1.5
2000
2020
2040
2060
2080
2100
SST mitigation, multi−model mean, A2 scenario
B
(ΔSST_E − ΔSST_W) / ΔSST_E (%)
50
40
30
20
10
0
−10
−20
−30
−40
2000
2020
2040
2060
2080
2100